

Flexophotovoltaic Effect and Above-Band-Gap Photovoltage Induced by Strain Gradients in Halide Perovskites

Zhiguo Wang,^{1,*} Shengwen Shu,^{2,*} Xiaoyong Wei,³ Renhong Liang,¹ Shanming Ke,¹
Longlong Shu,^{1,†} and Gustau Catalan^{4,5,‡}

¹*School of Physics and Materials Science, Nanchang University, Nanchang 330031, People's Republic of China*

²*College of Electrical Engineering and Automation, Fuzhou University, Fuzhou 350108, People's Republic of China*

³*Electronic Materials Research Laboratory, Key Laboratory of the Ministry of Education and International Center for Dielectric Research, Xi'an Jiao Tong University, Xi'an 710049, People's Republic of China*

⁴*Institució Catalana de Recerca i Estudis Avançats (ICREA), Barcelona 08010, Catalonia*

⁵*Institut Català de Nanociència i Nanotecnologia (ICN2), CSIC-BIST, Campus Universitat Autònoma de Barcelona, Barcelona 08193, Catalonia*



(Received 13 July 2023; accepted 5 December 2023; published 20 February 2024)

We have measured the flexophotovoltaic effect of single crystals of halide perovskites MAPbBr₃ and MAPbI₃, as well as the benchmark oxide perovskite SrTiO₃. For halide perovskites, the flexophotovoltaic effect is found to be orders of magnitude larger than for SrTiO₃, and indeed large enough to induce photovoltages bigger than the band gap. Moreover, we find that in MAPbI₃ the flexophotovoltaic effect is additional to a native bulk photovoltaic response that is switchable and ferroelectric-like. The results suggest that strain *gradient engineering* can be a powerful tool to modify the photovoltaic output even in already well-established photovoltaic materials.

DOI: [10.1103/PhysRevLett.132.086902](https://doi.org/10.1103/PhysRevLett.132.086902)

Photovoltaic effects require broken space-inversion symmetry, so that photogenerated carriers have a preferential direction in which to flow and thus establish a photocurrent [1–6]. In conventional solar cells, the spatial symmetry is broken by interfaces, and photocarriers flow towards the most charge-affine side of the junctions [5,6]. Spatial inversion symmetry is also inherently broken, without the need for interfaces, inside materials with piezoelectric crystal structures. Electron-hole pairs photogenerated inside piezoelectrics have different probabilities of drifting in opposite directions, thus generating a current in response to illumination. This later response is known as the “bulk photovoltaic effect,” and its magnitude does not abide by the same limits as junction solar cells; in particular, bulk photovoltages can be larger than the semiconductor band gap [1–3].

The space-inversion symmetry of any crystal, piezoelectric or otherwise, can also be broken by a strain gradient (a lattice curvature). This is the basis of flexoelectricity, a linear coupling between strain gradients and polarization that is allowed by symmetry in all materials [7], including semiconductors [8,9]. When strain gradients polarize a material, they enable a gradient-induced bulk photovoltaic effect known as the flexophotovoltaic effect [4]. Though some questions remain open about the flexophotovoltaic effect [10], the symmetry principle behind it is robust. On the other hand, while its existence is guaranteed from symmetry principles, its exact magnitude remains unknown

for most if not all materials. Connected to this question, it is also not known whether strain gradients alone can achieve the above-band-gap photovoltages that have so far been the exclusive preserve of piezoelectric materials [1,11] or tandem effects [12,13]. In this Letter, we quantify the flexophotovoltaic effect of some perovskites and show that it can indeed produce photovoltages bigger than the band gap. Specifically, we have measured the flexophotovoltaic effect of halide perovskites, a family of materials that combine high photovoltaic efficiency [6,14] and large flexoelectricity [15]. In addition, we have measured SrTiO₃ (STO), which is a benchmark oxide perovskite [16] and the first material in which the flexophotovoltaic effect was detected [4].

The halide-perovskite single crystals in this study were made by us (see Methods in the Appendix), and the STO crystals were commercially acquired (TOPVENDOR, Beijing, China). Identical Au electrodes were deposited on opposite sides of the crystals to make symmetric sandwich-capacitor structures [sketch in Fig. 1(a)], which were illuminated laterally so that, by symmetry, the possible photovoltaic contributions from opposite electrode interfaces mutually cancel. Illumination was provided by LED light with 405 nm wavelength for MAPbBr₃ (MAPB) and MAPbI₃ (MAPI), and 365 nm for STO, which has a larger band gap. The maximum light intensity was set to 1000 LUX, as calibrated at sample location using a photometer. The same photometer, in combination with

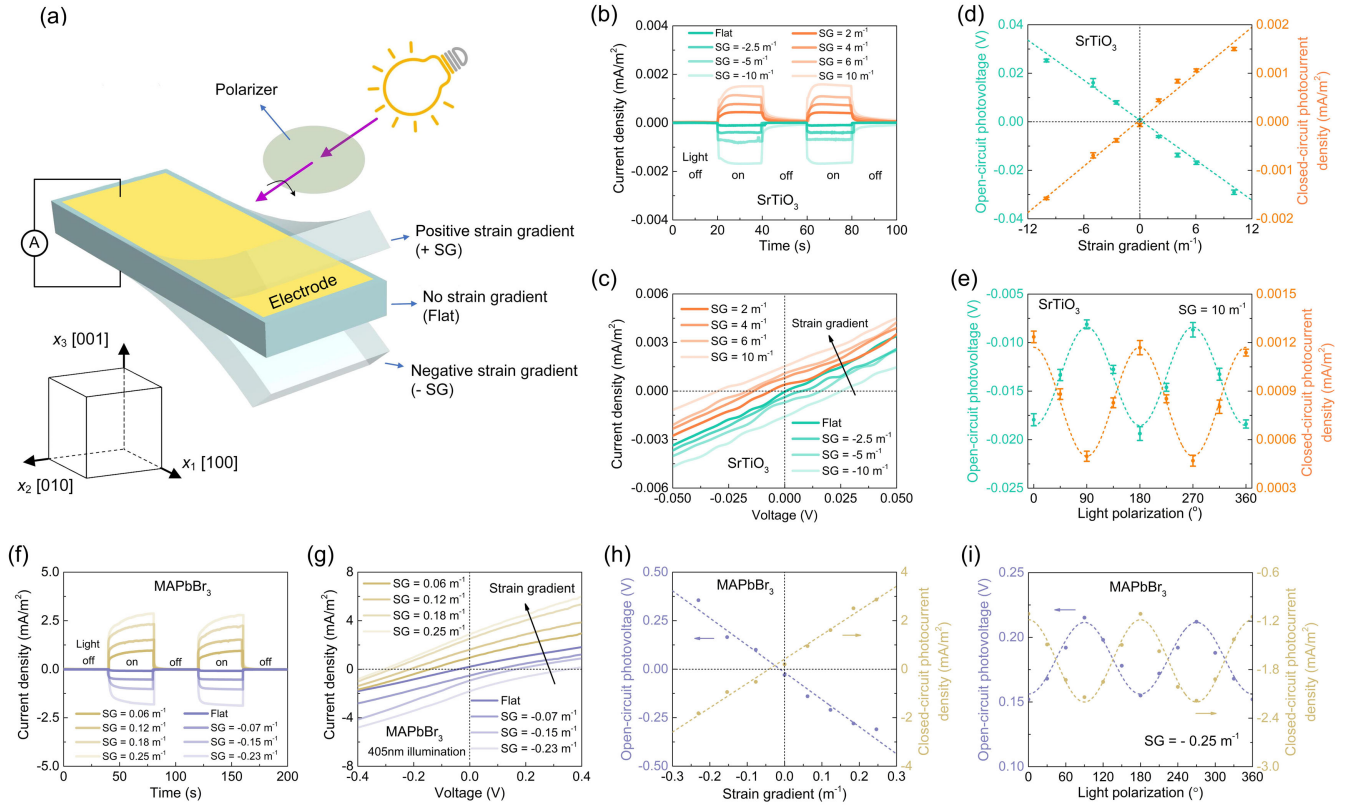


FIG. 1. Schematic configuration of flexophotovoltaic experiment and results for STO and MAPB. (a) Single crystals with identical top and bottom electrodes are clamped in the thickness direction [001] and bent vertically (see Supplemental Material, Fig. S2 [17]). The lower left shows the relation between coordinate axis and crystal direction. The crystals were bent around the [010] axis and illuminated laterally along the bending axis. A polarizing filter was introduced after the measurements in order to verify the bulk nature of the photoresponse. All measurements were performed under 1000 LUX of illuminance. (b) and (f) Photocurrent density as a function of applied strain gradient. (c) and (g) Current as a function of voltage under bending and illumination. (d) and (h) Open-circuit photovoltage (voltage for which there is no current) and closed-circuit photocurrent (current at 0 V) as a function of strain gradient, as extracted from 1(c) and 1(g) (example procedure provided in Supplemental Material [17], S3). (e) and (i) Photovoltage and photocurrent as a function of the polarization of the incident light with respect to the [001] direction, which is perpendicular to the electrodes and parallel to the flexoelectric polarization. The observed π -periodic response is consistent with a bulk photovoltaic effect.

a polarizer placed between the light source and sample was used to verify that the light emitted by the LED was not linearly polarized [less than 1% variation in incident light as a function of polarizer angle, see Supplemental Material [17], video S1]; this helps exclude artifacts from the dependence between photovoltaic output and polarization angle of incident light, which is a characteristic of the bulk photovoltaic effect [1,18]. To quantify the flexophotovoltaic effect, the crystals were bent in single-clamp cantilever geometry, and we used the standard continuum-mechanics equation of a bent beam to calculate the strain gradient from the vertical deflection [19]. The experimental scheme is depicted in Fig. 1(a) and further experimental details are provided in the Supplemental Material [17] (Fig. S2), which contains additional Refs. [20,21]. The currents are measured in steady state, and are therefore measured in steady state, and are therefore photovoltaic and not electromechanical (displacement current induced by change in deformation) nor pyroelectric (displacement

current induced by change in temperature). Photoflexoelectric [15] and pyroelectric effects are therefore excluded from these measurements.

Figure 1 shows the results for STO and MAPB, which are centrosymmetric at room temperature [22]. The current as a function of voltage under illumination was measured for various curvatures [Figs. 1(c) and 1(g) for STO and MAPB, respectively] and, from these, the open-circuit photovoltage and closed-circuit photocurrents were extracted and plotted [Figs. 1(d) and 1(h)], evidencing a linear dependence on strain gradient. In the absence of bending, the photocurrents of STO [Fig. 1(b)] and MAPB [Fig. 1(f)] are negligible, as expected (though not exactly zero as residual gradients, imperfect centering of the illumination, or slight differences between the surfaces are experimentally inevitable).

To quantify the flexophotovoltaic effect, we define the flexophotovoltage coefficient as $\Phi_V(\partial V_{OC}/\partial G)$, where V_{OC} is the open-circuit photovoltage, measured in volts

at 1000 LUX, and G is the strain gradient (curvature) measured in m^{-1} . Linear regression of the results in Figs. 1(d) and 1(h), respectively, yields $\Phi_V = -3 \times 10^{-3} \text{ V/m}^{-1}$ for STO and $\Phi_V = -1.3 \text{ V/m}^{-1}$ for MAPB, which is almost 3 orders of magnitude larger despite being measured in identical conditions. These results were reproducible in other crystals (see Supplemental Material [17], Fig. S4).

To date, there is no first-principles theory of the photoflexoelectric effect, making it impossible to compare these results to theoretical predictions. In the absence of a quantitative theory of the flexophotovoltaic effect, however, we can look at its closest relative, namely, the theory of the bulk photovoltaic effect [18,23,24]. This theory applies only to polar materials, but luckily there exist calculations for two polar relatives of the materials studied here: BaTiO_3 (ferroelectric) instead of SrTiO_3 , and MAPI (whose spontaneous polarization we examine later in this Letter) instead of MAPB. The ratio between the theoretical shift currents of these materials (10^{-3} – 10^{-5} mA/W for BTO [25] and ~ 0.1 – 1 mA/W for MAPI [26]) is similar to the ratio between photocurrent densities in our bent crystals, suggesting that the flexophotovoltaic effect can indeed be rationalized within a bulk photovoltaic framework, with the results being consistent with expectation for polarized perovskites, irrespective of whether the polarization is spontaneous (as in the theoretical calculations for the bulk photovoltaic effect) or induced (as in our experiment).

While it is tempting to attribute the difference to a larger flexoelectric coefficient of MAPB [15] compared to STO [16], it is worth mentioning that experimental flexoelectric coefficients are effective values that include both bulk and surface effects, with the latter being dominant in semiconductors [8]. In contrast, the flexophotovoltaic effect is a bulk one [4], and therefore the flexoelectricity that matters should not be the total one but only its bulk component. The bulk flexoelectric coefficient is unknown for halide perovskites, but for all materials it is proportional to the static dielectric constant [7,27], which is of the order of <100 for MAPB [15,28] compared to ~ 300 for STO [29]. We therefore think that the large flexophotovoltaic difference between these materials does not reflect their flexoelectric coefficients, but their optical properties. Specifically, the optical-frequency dielectric constant of halide perovskites [28] is higher than for STO [29], resulting in bigger screening and a more delocalized wave function, which is known to favor larger bulk photovoltaic effects [26], as well as longer carrier lifetimes and diffusion lengths—which are indeed much bigger for MAPB ($\sim 1 \mu\text{s}$ [30] and $>100 \mu\text{m}$ [31]) than for STO (60 ns [32] and $\sim 100 \text{ nm}$ [33]).

The above discussion assumes that the flexophotovoltaic effect is a bulk one, but this assumption needs to be verified. Although the photovoltaic contributions from

identical crystal-electrode interfaces should, by symmetry, mutually cancel when the crystal is flat, their equivalence is broken under bending, because one interface becomes compressed while the other is stretched, and differences in surface strain can modify the interfacial charge density via the deformation potential [15,34]. To determine the relative importance of bulk vs interfacial contributions, we have examined the dependence of the photovoltaic effect on the polarization angle of incident linearly-polarized light [Figs. 1(e) and 1(i)]. The observed 90° dependence of photovoltage and photocurrent on light-polarization angle is a signature of the bulk photovoltaic effect [1,4,18]. In addition, while the gold contacts were seen to become slightly rectifying under bending (Fig. S4-1 [17]), replacing Au by Ni, which remains Ohmic even under bending (Fig. S4-2 [17]), makes little difference to the flexophotovoltaic output. The results thus suggest that the perovskite-electrode interface does not play a relevant role in the measured flexophotovoltaic effect. Further proof of its bulk nature is provided by its bigger-than-bandgap magnitude, which we measured at the nanoscale and discuss later in this Letter.

Before moving onto nanoscale experiments, we completed the crystal-bending experiments by examining the generality of the flexophotovoltaic effect of halides, and whether it can coexist with other photovoltaic effects. For this, we look at MAPI, a halide perovskite controversially reported to be ferroelectric [35–37]. The flexophotovoltaic response of MAPI single crystals, made and measured following the same procedure as for MAPB, is shown in Figs. 2(a) and 2(b). The results show that indeed bending the crystal modifies the photovoltaic output, i.e., there is a flexophotovoltaic effect. However, unlike MAPB, MAPI already shows a significant photovoltage in the initial flat state. The bulk nature of the photovoltaic effect both in the

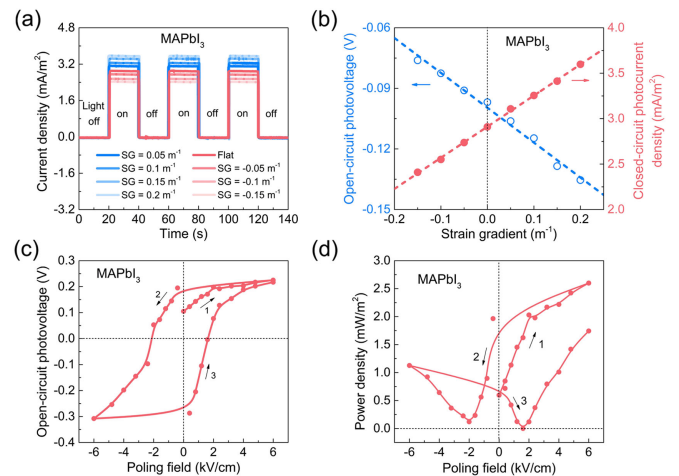


FIG. 2. Photovoltaic output of MAPI as a function of strain gradient (a),(b) and poling field (c),(d). The results show a native bulk photovoltaic effect that can be modified both by strain gradients and, hysteretically, by electric fields.

flat and in the bent states is supported by the 90° sinusoidal dependence of the photovoltage on the light polarization (Supplemental Material [17], Fig. S5). The results thus indicate *vis à vis* that the flexophotovoltaic effect can coexist with other bulk photovoltaic effects *and* that MAPI has a native bulk photovoltaic effect and is therefore polar even when flat.

We have characterized the switchability of the spontaneous bulk photovoltaic effect of MAPI by measuring the open-circuit photovoltage as a function of the pre-poling field. The results show a ferroelectriclike hysteresis [Figs. 2(c) and 2(d)]. Since the photovoltage and photocurrent have been measured after, not during, the application of the poling voltage, these hysteresis loops should be robust against the so-called “banana loop” artifact induced by leakage currents in semiconductors [38]. The observed photovoltaic hysteresis is thus indicative of a switchable macroscopic polarization, and is therefore functionally identical to what would be expected from a ferroelectric. On the other hand, while these macroscopic measurements evidence macroscopic polarization, they cannot by themselves determine the existence of ferroelectricity at the crystallographic unit-cell level. It is worth emphasizing this point because macroscopic polarization, induced by chemical or microstructural gradients, can exist in crystallographically nonpolar materials [39,40], and chemical gradients can exist in MAPI [41]. At any rate, the hysteretic dependence of photovoltaic output on poling history does show that poling voltage can tune the magnitude and sign of the photovoltaic output of MAPI just as it would in a ferroelectric material.

A distinct feature of the bulk photovoltaic effect is that it can yield photovoltages bigger than the band gap [1–3,25,26]. If the flexophotovoltaic effect of halide perovskites is a bulk phenomenon, then, sufficiently large strain gradients might be able to induce above-bandgap photovoltages. In our bending experiments, the maximum curvature of the crystals before breaking (0.25 m^{-1}) is insufficient to induce an above-bandgap photovoltage. However, larger strain gradients can be induced by working at smaller size scales [42,43], and, in particular, large local deformations can be induced by indentation using the sharp tip of an atomic force microscope (AFM) [4,44]. We therefore have used an AFM with a conductive tip to induce a large local strain gradient and collect the photovoltaic output as a function of vertical tip-force (Fig. 3). For this experiment, we have used microcrystals of only $\sim 1\ \mu\text{m}$ thickness to enhance the volume fraction of material under indentation. The crystals were made following a spin-coating method [45]. Micrographs of the crystals are provided in the Supplemental Material [17] S6, and an AFM topography map of the actual sample used in the experiment is shown in Fig. 3(b).

As shown in Fig. 3, the open-circuit photovoltage increases in direct proportion to the indentation force

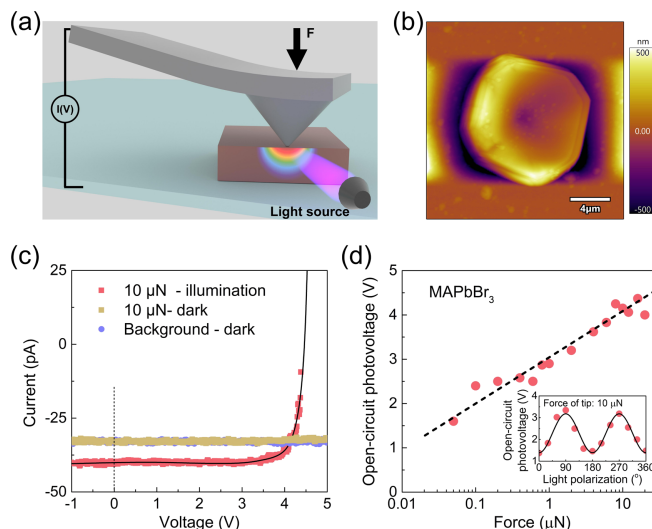


FIG. 3. Above-band-gap photovoltage induced by strain gradients. (a) Scheme of the experiment, whereby a large local curvature is induced by pushing with the tip of an atomic force microscope, and the current vs voltage is measured under illumination for various indentation forces. (b) Microcrystal used for the measurement. The thickness of the crystal is $\sim 1\ \mu\text{m}$ and the bottom electrode is ITO. We observed no mechanical damage to the sample even after applying a maximal indentation force of $20\ \mu\text{N}$ (see comparison in Supplemental Material [17], Fig. S6-2). (c) Current vs voltage measured under an indentation force of $10\ \mu\text{N}$, showing a $\sim 4\ \text{V}$ open-circuit photovoltage (d) open-circuit photovoltage as a function of indentation force (extracted from Fig. S7 [17]), showing the correlation between the two and (inset) photovoltage as a function of linear light-polarization angle, showing the same sinusoidal dependence as in the bulk crystals.

and therefore the strain gradient, surpassing the $2.3\ \text{eV}$ band gap and reaching $\sim 4\ \text{V}$ for applied forces of the order of $10\ \mu\text{N}$ [Figs. 3(c) and 3(d)]. Even larger photovoltages of up to $\sim 6\ \text{V}$ (more than twice the band gap) could be achieved at lower indentation forces by working with a sharper tip (Supplemental Material [17], S9 and S10). The photovoltaic output of the indentation experiment follows the 90° -degree sinusoidal dependence on light-polarization angle [inset of Fig. 3(d)], further supporting a bulk photovoltaic origin. The MAPB samples in which we have measured these results are single crystals and therefore lack grain boundaries that might otherwise act as tandem junctions [13]. The results thus demonstrate that above-band-gap photovoltage can be induced by the flexophotovoltaic effect alone in centrosymmetric materials.

This work was supported by the Natural Science Foundation of China (No. 12174174 and No. 51962020) and the Natural Science Foundation of Jiangxi Province (No. 20212ACB214011 and No. 20202ZDB01006). G. C. acknowledges financial support from Project PID2019–108573 GB-C21 funded by MCIN/AEI and a Severo

Ochoa Grant No. CEX2021-001214-S. He also thanks Professor Dennis Meier for hosting him as visiting professor at NTNU (Trondheim) during part of the time dedicated to this project; the stay at NTNU was partially funded by Grant No. PRX22/00595 from the Spanish Ministry of Universities. L. S. is thankful for the support from Nanchang University. We also thank Professor Massimiliano Stengel for stimulating discussions.

Appendix: Methods.—Sample information: STO (100) single crystals were commercially acquired from TOPVENDOR, with dimensions of 5 mm × 15 mm × 0.1 mm (width × length × thickness). The electrode dimensions are 5 mm × 4 mm (width × length).

MAPB single crystals for bending were prepared using the following raw materials: methylammonium bromide (CH₃NH₃Br, 99.5%, Advanced Election Technology), lead bromide (PbBr₂, 99.9%, Advanced Election Technology), N,N-dimethylformamide (DMF, 99%, Energy Chemical). MAPI single crystals for bending were prepared using the following raw materials: methylammonium iodine (CH₃NH₃I, 99.5%, Advanced Election Technology), lead iodine (PbI₂, 99.5%, Advanced Election Technology), γ -butyrolactone (GBL, $\geq 99\%$, Energy Chemical). MAPB and MAPI single crystals were grown using the inverse temperature crystallization method [44,46]. MAPB and MAPI single crystals were grown from its saturated solution in DMF and GBL (the concentration is 1 mol/L), respectively. We used 2000 mesh sandpaper to sand down the crystals to a lower thickness, followed by polishing the top and bottom surfaces with finer sandpaper (first 5000 mesh, then 10000 mesh) to achieve a mirror-smooth surface. The final dimensions of the MAPB single crystals were 5 mm × 15 mm × 1 mm, and MAPI crystals were 5 mm × 15 mm × 0.9 mm. The electrodes were 5 mm × 4 mm (width × length) for both.

MAPB microcrystals for AFM experiment: Following Ref. [45], the MAPB solution (1 mol/L) was spin coated at 2000 rpm/min for 30 s on the glass with the indium tin oxide (ITO) electrode. Heating treatment at 70 °C for 30 min was carried out after the spin-coating process. Figure S5 shows the single-crystal morphology of the MAPB microcrystals. The thickness of the micro MAPB single crystals was ~ 1 μm (Fig. S6-2) [17].

Illumination: The photovoltaic response was induced using a nonpolarized LED light source (Model: HY-UV0003). The illuminance on the sample was measured using a photometer (Model: DT1330A, LIHUAJIN). The nonpolarized nature of the light was verified by measuring the intensity of the incident light as a function of polarizer angle; luminance variations as a function of polarizer rotation were smaller than 1% (see Supplemental Material [17], S1).

Strain gradients: The rectangular-beam-shaped crystals were clamped at one end and pushed at the opposite free end to induce single-clamp cantilever bending. The free end was pushed from above or from below to induce positive or negative strain gradients, respectively. In single-clamp cantilever geometry, the strain gradient was calculated from the vertical deflection of the free end using this equation [19]:

$$\frac{\partial \varepsilon_{11}}{\partial x_3} = \frac{3w(L)}{L^2} \left(1 - \frac{x}{L}\right), \quad (\text{A1})$$

where $w(L)$ is the vertical deflection delivered by the piezoelectric actuator at the end of the cantilever, L is the length of the cantilever, and x is the horizontal position from the center of the electrode to the fixed end, respectively.

Atomic force microscopy: The electrical-transport characterization of MAPB single crystal under a tip force was measured using a Cypher ES (Asylum Research) atomic force microscope with ORCA mode (conductive AFM). A diamond-coated conductive probe (Model: CDT-NCLR) with a diameter of ~ 150 nm and force constants of 72 N m⁻¹ was used to apply pressure to the MAPbBr₃ single crystal, and the current-voltage (I - V) curve of the crystal was measured at the same time. An electrical bias was applied through the substrate, which was swiped at a ramping rate ~ 1 V s⁻¹. The background noise was lower than ± 50 pA in the 20 nA measurement range. The AFM tips were calibrated by the thermal noise method, which allows us to precisely obtain the inverse optical lever sensitivity (InvOLS) and the spring constant of the tips. The mechanical force was calculated by multiplying the spring constant, InvOLS and cantilever deflection [force = spring constant × InvOLS × (preset deflection – initial deflection)]. All measurements were performed in air at room temperature.

The measurement protocol was as follows: (1) The AFM tip was placed in contact with the surface of the crystal with a preset force. (2) After the applied force reached a preset value, the compressive force was maintained constant by the feedback amplifier circuit of the controller, and then the electrical measurements were initiated. In this stage, a sweeping bias voltage was applied between the substrate and the tip, and the current was measured. (3) After each I - V measurement, a new compressive force was applied and the corresponding electrical measurement was performed. (4) In addition, we measured the time dependence of photocurrent and photovoltage for given mechanical set points. The results, shown in the Supplemental Material [17], Fig. S8, show that the steady-state values do not differ significantly from those measured in the I - V cycles.

*These authors contributed equally to this work.

†llshu@ncu.edu.cn

‡gustau.catalan@icn2.cat

- [1] V. M. Fridkin, Bulk photovoltaic effect in noncentrosymmetric crystals, *Crystallogr. Rep. (Transl. Kristallografiya)* **46**, 654 (2001).
- [2] I. Grinberg, D. V. West, M. Torres, G. Y. Gou, D. M. Stein, L. Y. Wu, G. N. Chen, E. M. Gallo, A. R. Akbashev, P. K. Davies, J. E. Spanier, and A. M. Rappe, Perovskite oxides for visible-light-absorbing ferroelectric and photovoltaic materials, *Nature (London)* **503**, 509 (2013).
- [3] A. Pusch, U. Römer, D. Culcer, and J. E. D. Nicholas, Energy conversion efficiency of the bulk photovoltaic effect, *PRX Energy* **2**, 013006 (2023).
- [4] M. M. Yang, D. J. Kim, and M. Alexe, Flexo-photovoltaic effect, *Science* **360**, 904 (2018).
- [5] W. Shockley and H. J. Queisser, Detailed balance limit of efficiency of p-n junction solar cells, *J. Appl. Phys.* **32**, 510 (1961).
- [6] J. Y. Kim, J. W. Lee, H. S. Jung, H. Shin, and N. G. Park, High-efficiency perovskite solar cells, *Chem. Rev.* **120**, 7867 (2020).
- [7] P. Zubko, G. Catalan, and A. K. Tagantsev, Flexoelectric effect in solids, *Annu. Rev. Mater. Res.* **43**, 387 (2013).
- [8] J. Narvaez, F. Vasquez-Sancho, and G. Catalan, Enhanced flexoelectric-like response in oxide semiconductors, *Nature (London)* **538**, 219 (2016).
- [9] L. F. Wang, S. H. Liu, X. L. Feng, C. L. Zhang, L. P. Zhu, J. Y. Zhai, Y. Qin, and Z. L. Wang, Flexoelectronics of centrosymmetric semiconductors, *Nat. Nanotechnol.* **15**, 661 (2020).
- [10] H. Y. Zou, C. L. Zhang, H. Xue, Z. Y. Wu, and Z. L. Wang, Boosting the solar cell efficiency by flexo-photovoltaic effect?, *ACS Nano* **13**, 12259 (2019).
- [11] A. Pérez-Tomás, M. Lira-Cantú, and G. Catalan, Above-bandgap photovoltages in antiferroelectrics, *Adv. Mater.* **28**, 9644 (2016).
- [12] S. Y. Yang, J. Seidel, S. J. Byrnes, P. Shafer, C.-H. Yang, M. D. Rossell, P. Yu, Y.-H. Chu, J. F. Scott, J. W. Ager, III, L. W. Martin, and R. Ramesh, Above-bandgap voltages from ferroelectric photovoltaic devices, *Nat. Nanotechnol.* **5**, 143 (2010).
- [13] Y. B. Yuan, T. Li, Q. Wang, J. Xing, A. Gruverman, and J. S. Huang, Anomalous photovoltaic effect in organic-inorganic hybrid perovskite solar cells, *Sci. Adv.* **3**, e1602164 (2017).
- [14] J. Burschka, N. Pellet, S. J. Moon, R. Humphry-Baker, P. Gao, M. K. Nazeeruddin, and M. Grätzel, Sequential deposition as a route to high-performance perovskite-sensitized solar cells, *Nature (London)* **499**, 316 (2013).
- [15] L. L. Shu, S. M. Ke, L. F. Fei, W. B. Huang, Z. G. Wang, J. H. Gong, X. N. Jiang, L. Wang, F. Li, S. J. Lei, Z. G. Rao, Y. B. Zhou, R. K. Zheng, X. Yao, Y. Wang, M. Stengel, and G. Catalan, Photoflexoelectric effect in halide perovskites, *Nat. Mater.* **19**, 605 (2020).
- [16] P. Zubko, G. Catalan, A. Buckley, P. R. L. Welche, and J. F. Scott, Strain-gradient-induced polarization in SrTiO₃ single crystals, *Phys. Rev. Lett.* **99**, 167601 (2007).
- [17] See Supplemental Material at <http://link.aps.org/supplemental/10.1103/PhysRevLett.132.086902> for complementary experiments described in the paper and photographs of the experimental setup and the samples used.
- [18] R. Vonbaltz and W. Kraut, Theory of the bulk photovoltaic effect in pure-crystals, *Phys. Rev. B* **23**, 5590 (1981).
- [19] L. B. Zhang, Z. G. Wang, S. W. Shu, Y. M. Hu, C. C. Li, S. M. Ke, F. Li, and L. L. Shu, Origin of defects-induced large flexoelectricity in ferroelectric ceramics, *Phys. Rev. Mater.* **6**, 094416 (2022).
- [20] F. C. Cui, P. Zhang, L. Z. Zhang, Y. Q. Hua, X. Sun, X. Li, G. D. Zhang, and X. T. Tao, Liquid phase epitaxial growth of large-area MAPbBr₃ - nCln/CsPbBr₃ perovskite single-crystal heterojunction for enhancing sensitivity and stability of x-ray detector, *Chem. Mater.* **34**, 9601 (2022).
- [21] M. Lomonosov, X. L. Yan, C. X. Sheng, V. E. Gusev, C. Y. Ni, and Z. Shen, Exceptional elastic anisotropy of hybrid organic-inorganic perovskite CH₃NH₃PbBr₃ measured by laser ultrasonic technique, *Phys. Status Solidi RRL* **10**, 606 (2016).
- [22] H. Wang, R. H. Nan, Z. Y. Jian, C. Q. Jin, Y. X. Wei, Y. P. Bai, and H. L. Li, Step-controlled growth of MAPbBr₃ single crystal and temperature-dependent variations of MA⁺ cations during nonphase transition, *Mater. Sci. Semicond. Process.* **135**, 106107 (2021).
- [23] V. I. Belinicher and B. I. Sturman, The photogalvanic effect in media lacking a center of symmetry, *Sov. Phys. Usp.* **23**, 199 (1980).
- [24] W. Ruppel, R. Vonbaltz, and P. Wurfel, The origin of the photo-EMF in ferroelectric and non-ferroelectric materials, *Ferroelectrics* **43**, 109 (1982).
- [25] C. Paillard, X. F. Bai, I. C. Infante, M. Guennou, G. Geneste, M. Alexe, J. Kreisel, and B. Dkhil, Photovoltaics with ferroelectrics: Current status and beyond, *Adv. Mater.* **28**, 5153 (2016).
- [26] L. Z. Tan, F. Zheng, S. M. Young, F. G. Wang, S. Liu, and A. M. Rappe, Shift current bulk photovoltaic effect in polar materials—hybrid and oxide perovskites and beyond, *npj Comput. Mater.* **2**, 16026 (2016).
- [27] A. K. Tagantsev, Piezoelectricity and flexoelectricity in crystalline dielectrics, *Phys. Rev. B* **34**, 5883 (1986).
- [28] S. Govinda, B. P. Kore, M. Bokdam, P. Mahale, A. Kumar, S. Pal, B. Bhattacharyya, J. Lahnsteiner, G. Kresse, C. Franchini, A. Pandey, and D. D. Sarma, Behavior of methylammonium dipoles in MAPbX₃ (X = Br and I), *J. Phys. Chem. Lett.* **8**, 4113 (2017).
- [29] I. Fedorov *et al.*, Far-infrared spectroscopy of a SrTiO₃ thin film, *Ferroelectrics*, *Ferroelectrics* **208–209**, 413 (1998).
- [30] D. Shi, V. Adinolfi, R. Comin, M. J. Yuan, E. Alarousu, A. Buin, Y. Chen, S. Hoogland, A. Rothenberger, K. Katsiev, Y. Losovyj, X. Zhang, P. A. Dowben, O. F. Mohammed, E. H. Sargent, and O. M. Bakr, Low trap-state density and long carrier diffusion in organolead trihalide perovskite single crystals, *Science* **347**, 519 (2015).
- [31] B. Turedi, M. N. Lintangpradipto, O. J. Sandberg, A. Yazmaciyan, G. J. Matt, A. Y. Alsalloum, K. Almasabi, K. Sakhatskyi, S. Yakunin, X. P. Zheng, R. Naphade,

- S. Nematullov, V. Yeddu, D. Baran, A. Armin, M. I. Saidaminov, M. V. Kovalenko, O. F. Mohammed, and O. M. Bakr, Single-crystal perovskite solar cells exhibit close to half a millimeter electron-diffusion length, *Adv. Mater.* **34**, 2202390 (2022).
- [32] M. Kato and Y. Kato, Estimation of surface recombination velocities and bulk carrier lifetime for SrTiO₃ using angle-lapped structures, *Chem. Phys. Lett.* **805**, 139955 (2022).
- [33] M. Kissel, L. Porz, T. Frömling, A. Nakamura, J. Rödel, and M. Alexe, Enhanced photoconductivity at dislocations in SrTiO₃, *Adv. Mater.* **34**, 2203032 (2022).
- [34] M. Stengel, Surface control of flexoelectricity, *Phys. Rev. B* **90**, 201112(R) (2014).
- [35] S. Shahrokhi, W. X. Gao, Y. T. Wang, P. R. Anandan, M. Z. Rahaman, S. Singh, D. Y. Wang, C. Cazorla, G. L. Yuan, J. M. Liu, and T. Wu, Emergence of ferroelectricity in halide perovskites, *Small Methods* **4**, 2000149 (2020).
- [36] M. N. F. Hoque, M. J. Yang, Z. Li, N. Islam, X. Pan, K. Zhu, and Z. Y. Fan, Polarization and dielectric study of methylammonium lead Iodide thin film to reveal its nonferroelectric nature under solar cell operating conditions, *ACS Energy Lett.* **1**, 142 (2016).
- [37] I. Anusca, S. Balciunas, P. Gemeiner, S. Svirskas, M. Sanlialp, G. Lackner, C. Fettkenhauer, J. Belovickis, V. Samulionis, M. Ivanov, B. Dkhil, J. Banys, V. V. Shvartsman, and D. C. Lupascu, Dielectric response: Answer to many questions in the methylammonium lead halide solar cell absorbers, *Adv. Energy Mater.* **7**, 1700600 (2017).
- [38] J. F. Scott, Ferroelectrics go bananas, *J. Phys. Condens. Matter* **20**, 021001 (2008).
- [39] A. Biancoli, C. M. Fancher, J. L. Jones, and D. Damjanovic, Breaking of macroscopic centric symmetry in paraelectric phases of ferroelectric materials and implications for flexoelectricity, *Nat. Mater.* **14**, 224 (2015).
- [40] O. Aktas, M. Kangama, G. Linyu, G. Catalan, X. D. Ding, A. Zunger, and E. K. H. Salje, Piezoelectricity in nominally centrosymmetric phases, *Phys. Rev. Res.* **3**, 043221 (2021).
- [41] Z. G. Xiao, Y. B. Yuan, Y. C. Shao, Q. Wang, Q. F. Dong, C. Bi, P. Sharma, A. Gruverman, and J. S. Huang, Giant switchable photovoltaic effect in organometal trihalide perovskite devices, *Nat. Mater.* **14**, 193 (2015).
- [42] T. D. Nguyen, S. Mao, Y. W. Yeh, P. K. Purohit, and M. C. McAlpine, Nanoscale flexoelectricity, *Adv. Mater.* **25**, 946 (2013).
- [43] Q. Deng, M. Kammoun, A. Erturk, and P. Sharma, Nanoscale flexoelectric energy harvesting, *Int. J. Solids Struct.* **51**, 3218 (2014).
- [44] H. Lu, C. W. Bark, D. E. Ojos, J. Alcala, C. B. Eom, G. Catalan, and A. Gruverman, Mechanical writing of ferroelectric polarization, *Science* **336**, 59 (2012).
- [45] R. García-Aboal, R. Fenollosa, F. Ramiro-Manzano, I. Rodríguez, F. Meseguer, and P. Atienzar, Single crystal growth of hybrid lead bromide perovskites using a spin-coating method, *ACS Omega* **3**, 5229 (2018).
- [46] M. I. Saidaminov, A. L. Abdelhady, B. Murali, E. Alarousu, V. M. Burlakov, W. Peng, I. Dursun, L. F. Wang, Y. He, G. Maculan, A. Goriely, T. Wu, O. F. Mohammed, and O. M. Bakr, High-quality bulk hybrid perovskite single crystals within minutes by inverse temperature crystallization, *Nat. Commun.* **6**, 7586 (2015).